2022

Performance Improvement of Lithium Metal Batteries Enabled By LiBF3CN as a New Electrolyte Additive

Oh B. Chae
University of Rhode Island

Venkata A.K. Adiraju
University of Rhode Island

Brett L. Lucht
University of Rhode Island, blucht@uri.edu

Citation/Publisher Attribution

Chae, O. B., Adiraju, V. A.K., & Lucht, B. L. (2022). Performance Improvement of Lithium Metal Batteries Enabled By LiBF3CN as a New Electrolyte Additive. *Journal of The Electrochemical Society, 169*(11), 110506. https://doi.org/10.1149/1945-7111/ac9d67
Available at: https://doi.org/10.1149/1945-7111/ac9d67

Performance Improvement of Lithium Metal Batteries Enabled By LiBF3CN as a New Electrolyte Additive

OPEN ACCESS

Performance Improvement of Lithium Metal Batteries Enabled By $LiBF_3CN$ as a New Electrolyte Additive

To cite this article: Oh B. Chae *et al* 2022 *J. Electrochem. Soc.* **169** 110506

Journal of The Electrochemical Society, 2022 **169** 110506

Performance Improvement of Lithium Metal Batteries Enabled By $LiBF_3CN$ as a New Electrolyte Additive

Oh B. Chae, Venkata A. K. Adiraju, and Brett L. Lucht[*,z]

Department of Chemistry, University of Rhode Island, Kingston, Rhode Island 02881, United States of America

A newly synthesized electrolyte additive, lithium trifluoro(cyano) borate ($LiBF_3CN$), has been investigated for electrochemical performance improvement of lithium metal batteries. The $LiBF_3CN$ has a structure where one fluorine atom of BF_4^- is substituted with a cyano group (−CN) prepared by the reaction of boron trifluoride etherate with lithium cyanide. The electrochemical performance in symmetric Li/Li cells and NCM523/Li cells is significantly improved upon the incorporation of $LiBF_3CN$ as an electrolyte additive into a carbonate-based electrolyte. Extensive characterization of the deposited lithium metal reveals that a thin (≈20 nm) and robust SEI composed of LiN_xO_y, Li_3N and Li_2O is formed by the reductive decomposition of the $LiBF_3CN$ additive, which plays an important role in decreasing the resistance and stabilizing lithium deposition/stripping. The insight into the substitution effect of a functional group obtained from this work provides guidance for the design of new electrolyte additives.
 [DOI: 10.1149/1945-7111/ac9d67]

Manuscript submitted August 17, 2022; revised manuscript received September 19, 2022. Published November 3, 2022. *This paper is part of the JES Focus Issue on Selected Papers from IMLB 2022.*

Supplementary material for this article is available online

Lithium metal is considered to be an excellent negative electrode material for next-generation high energy density batteries since it has ten times higher theoretical capacity (3860 mAh g^{-1}) than the currently commercialized graphite (372 mAh g^{-1}). Additionally, the low operating potential (−3.04 V vs standard hydrogen electrode) and low gravimetric density (0.534 g cm^{-3}) are very attractive for high energy density batteries.[1–5] Despite the exceptional properties of lithium metal, practical application is hindered by serious problems caused by lithium dendrite formation during lithium deposition/stripping.[6–8] Unlike the graphite anode which undergoes lithium intercalation/deintercalation for energy storage/release, the lithium metal anode requires deposition/stripping, causing a repeated change of the interface between lithium and the electrolyte during cycling. Thus, the role of electrolyte and solid electrolyte interphase (SEI) is more important for the reversible cycling of lithium metal anodes.[9–16] Recently, many strategies using electrolyte additives such as fluoroethylene carbonate (FEC),[17–19] lithium nitrate ($LiNO_3$),[20,21] lithium difluoro(oxalato)borate (LiDFOB),[22–24] lithium tetrafluoroborate ($LiBF_4$)[25,26] and multi-functional new additives[27,28] have been proposed for improving the electrochemical performance of lithium metal anodes. Among them, $LiBF_4$ has been primarily investigated as an electrolyte salt in lithium ion batteries due to its many favorable features including a lower charge transfer resistance at low temperature, good thermal stability, and less moisture sensitivity.[29,30] However, $LiBF_4$ has rarely been used in lithium ion batteries due to the relatively low lithium ion conductivity.[31,32] Instead of using $LiBF_4$ as the main electrolyte salt, it has also been reported to be used as an electrolyte additive.[26,33]

In this study, a new electrolyte additive, lithium trifluoro(cyano) borate ($LiBF_3CN$) has been synthesized and its electrochemical features have been evaluated in carbonate-based electrolyte for lithium metal batteries. In order to investigate the effect of substituting a cyano group (−CN) for one fluorine atom of BF_4^-, the electrochemical performance of $LiBF_3CN$ has been compared to $LiBF_4$. The electrochemical performance evaluations using symmetric Li/Li cells and NCM523/Li cells illustrate that the $LiBF_3CN$-containing electrolyte affords significantly improved cycling stability and rate capability. In particular, NCM523/Li cells with the $LiBF_3CN$-containing electrolyte exhibit excellent capacity retention with 98.4% after 300 cycles whereas the cells with the $LiBF_4$-containing electrolyte have poor capacity retention of 83.1% after 300 cycles. Various characterizations of the deposited lithium morphology and the SEI film have been carried out using field-emission scanning electron microscopy (FE-SEM), cryogenic transmission electron microscopy (cryo-TEM), and X-ray photoelectron spectroscopy (XPS), suggesting the generation of a thin (≈20 nm) and robust SEI film including N-compounds (LiN_xO_y, Li_3N) and Li_2O on the deposited lithium metal by reductive decomposition of $LiBF_3CN$ and carbonate solvents. The favorable SEI layer plays an important role in the decrease of interfacial resistance and the stable lithium deposition/stripping, resulting in superior electrochemical performance.

Experimental

Synthesis of lithium trifluoro(cyano) borate.—Lithium trifluoro (cyano) borate ($LiBF_3CN$) was synthesized through the following procedures. Boron trifluoride diethyl ether complex (48% BF_3) and solvents were purchased from Acros Organics and used as received. Lithium cyanide was prepared via the literature procedure.[34] At room temperature, boron trifluoride diethyl ether (0.27 ml, 21.1 mmol) was added dropwise to a solution of lithium cyanide (33 mg, 10.1 mmol) in anhydrous THF. The pale-yellow solution was stirred overnight and then the volatiles were removed in vacuo. To the obtained residue, dimethyl carbonate (1 ml), toluene (2 ml) and hexane (2 ml) were added and stirred resulting in a white precipitate. The solvent was decanted. Obtained precipitate was washed with toluene and dried overnight in vacuo to obtain white powder. Yield: 490.0 mg, 48%. $^{11}B\{^1H\}$ NMR (128 MHz, acetone-d_6) δ −1.1 (b); ^{19}F NMR (376 MHz, acetone-d_6) δ −153.59(s), −153.64(s).

Materials characterization.—^{11}B and ^{19}F nuclear magnetic resonance (NMR) spectra were obtained by using Bruker Ascend 400 MHz spectrometer. Field emission scanning electron microscopy (FE-SEM, Zeiss Sigma) was used to observe the deposited lithium metal morphology. X-ray photoelectron spectroscopy (XPS) measurements were performed using a K-alpha spectrometer (Thermo Scientific) to examine the surface film of lithium metal. The X-ray spot size and pass energy were 400 μm and 50 eV, respectively. The binding energy was corrected based on the C 1s spectrum, assigning hydrocarbon to 284.8 eV. The lithium metal electrodes for FE-SEM and XPS measurements were prepared as

*Electrochemical Society Member.
[z]E-mail: blucht@uri.edu

follows. The cells were disassembled after cycling, and the electrode samples were harvested in the Ar-filled dry box. To remove the residual electrolyte, the electrodes were washed with DMC (dimethyl carbonate) and dried overnight under vacuum. Cryogenic transmission electron microscopy (cryo-TEM) measurements were carried out using a JEOL JEM-2100F at 200 kV, equipped with a LaB_6 electron emission source. To prepare the cryo-TEM samples, 300 mesh TEM grids were placed on a copper foil working electrode and assembled with lithium metal foil counter electrode. After lithium was deposited on the TEM grid, the cells were disassembled and TEM grid was collected and washed with DMC in the Ar-filled dry box and dried overnight under vacuum. The dried TEM grid was quickly transferred into the TEM chamber using a cryo-transfer holder (Gatan). The TEM images were acquired at cryogenic temperature (−180 °C), which avoid beam damage to the samples.

Electrochemical measurements.—To prepare NCM523 electrodes, the $LiNi_{0.5}Co_{0.2}Mn_{0.3}O_2$ powder (MTI Corporation) was dispersed in *N*-methyl pyrrolidone with Super C as carbon additive and poly(vinylidenefluoride) (PVdF) as polymeric binder (90:5:5 in wt%). The resulting slurry was coated on aluminum foil that was used as current collector. The electrode was pressed with a roll presser and dried in a vacuum oven at 110 °C for overnight. The areal capacity of NCM523 electrodes was ca. 1.0 mAh cm^{-2}. The electrolyte with lithium tetrafluoroborate ($LiBF_4$) additive or lithium trifluoro(cyano) borate ($LiBF_3CN$) additive was prepared by adding $LiBF_4$ powder (5 wt%) or $LiBF_3CN$ powder (5 wt%) to baseline electrolyte which is 1 M lithium hexafluorophosphate ($LiPF_6$) in a mixture of ethylene carbonate (EC) and ethyl methyl carbonate (EMC) (3:7, v/v), and stirred overnight. For the symmetric Li/Li cell test, coin-type cells (2032-type) were fabricated for each electrolyte (100 μl) in Ar-filled dry box with lithium foil (0.75 mm thick, MTI Corporation) as a working/counter electrode and a PP/PE/PP separator (25 μm thick, Celgard 2325). To prepare the NCM523/Li cell, coin-type cells (2032-type) were fabricated for each electrolyte (100 μl) in Ar-filled dry box with lithium foil as an anode, NCM523 as a cathode and a PP/PE/PP separator was used. For the electrochemical tests, an Arbin BT2000 battery cycler was used at room temperature (25 °C) in a constant temperature oven. The symmetric Li/Li cells were cycled at a current density of 1 mA cm^{-2} for an areal capacity of 1 mAh cm^{-2} and at a current density of 2 mA cm^{-2} for an areal capacity of 1 mAh cm^{-2}, respectively. The NCM523/Li cells were cycled at a current density of 0.5 C (1 C = 155 mA g^{-1}) in a voltage range of 3.0–4.2 V (vs Li/Li^+). The rate performance tests of NCM523/Li cells were carried out at a voltage range of 3.0–4.2 V (vs Li/Li^+) in various current density of 0.2, 0.5, 1, 2, 5 and 0.2 C. For electrochemical impedance spectroscopy (EIS) measurements, BioLogic VSP was used in the frequency range of 0.5 MHz to 0.1 Hz with an amplitude of 10 mV.

Results and Discussion

Synthesis and characterization of $LiBF_3CN$.—A new electrolyte additive, $LiBF_3CN$, has been prepared by the reaction of boron trifluoride etherate with lithium cyanide as shown in Scheme 1. Boron trifluoride etherate was added slowly to a lithium cyanide solution in tetrahydrofuran (THF) at room temperature to generate a pale-yellow solution. A mixture of dimethyl carbonate, toluene and hexane was added to the solution resulting in the formation of a white precipitate. After the solvents were removed in vacuo, a white powder was obtained in 48% yield. The obtained lithium salt was characterized by ^{19}F (Fig. 1a) and $^{11}B\{^1H\}$ (Fig. 1b) NMR spectroscopy. The reaction of one equivalent of boron trifluoride with cyanide anion forms a boron salt containing a single cyanide group whereas the reaction of cyanide anion with excess of boron trifluoride forms disproportionation products.[35,36] It is noteworthy that the potassium salt of trifluro(cyano)borate anion has been previously reported.[37]

Electrochemical performance.—To compare the electrochemical performance between the 5 wt% of $LiBF_4$-containing electrolyte and the 5 wt% of $LiBF_3CN$-containing electrolyte, electrochemical investigation of symmetric Li/Li cells and NCM523/Li cells has been conducted. Typical galvanostatic cycling performance obtained for symmetric Li/Li cells cycled with the two different electrolyte systems are provided in Figs. 2a, 2b. The deposition and stripping cycling results of Li/Li cells at a current density of 1 mA cm^{-2} for areal capacity of 1 mAh cm^{-2} (Fig. 2a) reveal that the cells with $LiBF_3CN$-containing electrolyte have more stable cycling with lower overpotential than the cells with $LiBF_4$-containing electrolyte. The stable cycling of the cells with the $LiBF_3CN$-containing electrolyte is prolonged to 650 h while the cells with the $LiBF_4$-containing electrolyte have a sharp voltage increase and cell failure after 400 h. The cycling results at a higher current density of 2 mA cm^{-2} also reveal that the $LiBF_3CN$-containing electrolyte has better cycling performance than the $LiBF_4$-containing electrolyte. Although initial overpotentials in both cells are similar, the difference increases during cycling. The cells with $LiBF_4$-containing electrolyte exhibit a sharp increase in overpotential after 100 h. However, the cells with $LiBF_3CN$-containing electrolyte retain stable cycling with a smaller overpotential for almost 200 h. Moreover, the favorable performance of $LiBF_3CN$-containing electrolyte is further supported by electrochemical impedance spectroscopy (EIS) of symmetric Li/Li cells after 3 cycles which are provided in Fig. 2c. The spectra have the Ohmic resistance originated from electrolyte in the high frequency region and the following overlapped semicircles represent the interfacial resistance including the SEI and charge transfer resistances at the surface of the Li metal. The cells with $LiBF_3CN$-containing electrolyte have smaller Ohmic and interfacial resistances than the cells with $LiBF_4$-containing electrolyte. In addition, the surface of lithium metal cycled with $LiBF_4$-containing electrolyte after 100 cycles at 1 mA cm^{-2} for 1 mAh cm^{-2} has a porous and rough morphology with many dead lithium particles on the surface as depicted in Figs. 2d and S1a. In contrast, the lithium metal cycled with $LiBF_3CN$-containing electrolyte (Figs. 2e and S1b) has a denser and smoother surface morphology.

To further demonstrate the practicality of $LiBF_3CN$-containing electrolyte for applications in lithium metal batteries, NCM523/Li cells were fabricated, and their electrochemical performance was evaluated, which is provided in Fig. 3. The galvanostatic cycling performance of NCM523/Li cells at a current density of 0.5 C (Fig. 3a) shows that the cells with $LiBF_4$-containing electrolyte exhibit an abrupt sharp capacity loss after 100 cycles, and poor capacity retention of only 83.1% after 300 cycles. In comparison, the NCM523/Li cells with $LiBF_3CN$-containing electrolyte have very stable Coulombic efficiency and significantly improved capacity retention of 98.4% after 300 cycles. Furthermore, the corresponding voltage profiles in Figs. 3b and 3c, along with the dQ/dV plots in Figs. S2 and S3, provide additional insight into the electrochemical charge and discharge behaviors for both electrolyte systems. The cells with $LiBF_3CN$-containing electrolyte have low overpotential and very stable charge/discharge voltage profiles for 300 cycles whereas the cells with $LiBF_4$-containing electrolyte exhibit unstable

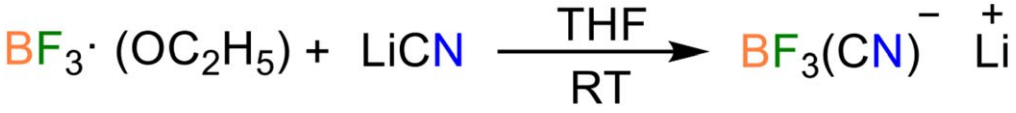

Scheme 1. Synthesis processes of lithium trifluoro(cyano) borate ($LiBF_3CN$).

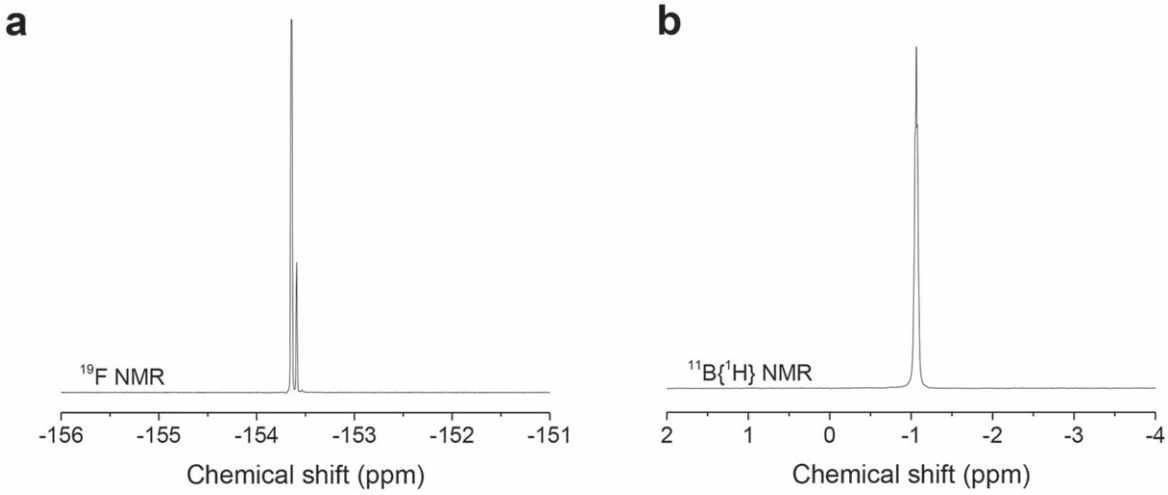

Figure 1. (a) ^{19}F NMR and (b) ^{11}B{^{1}H} NMR spectra of $LiBF_3CN$ powder in acetone-d6.

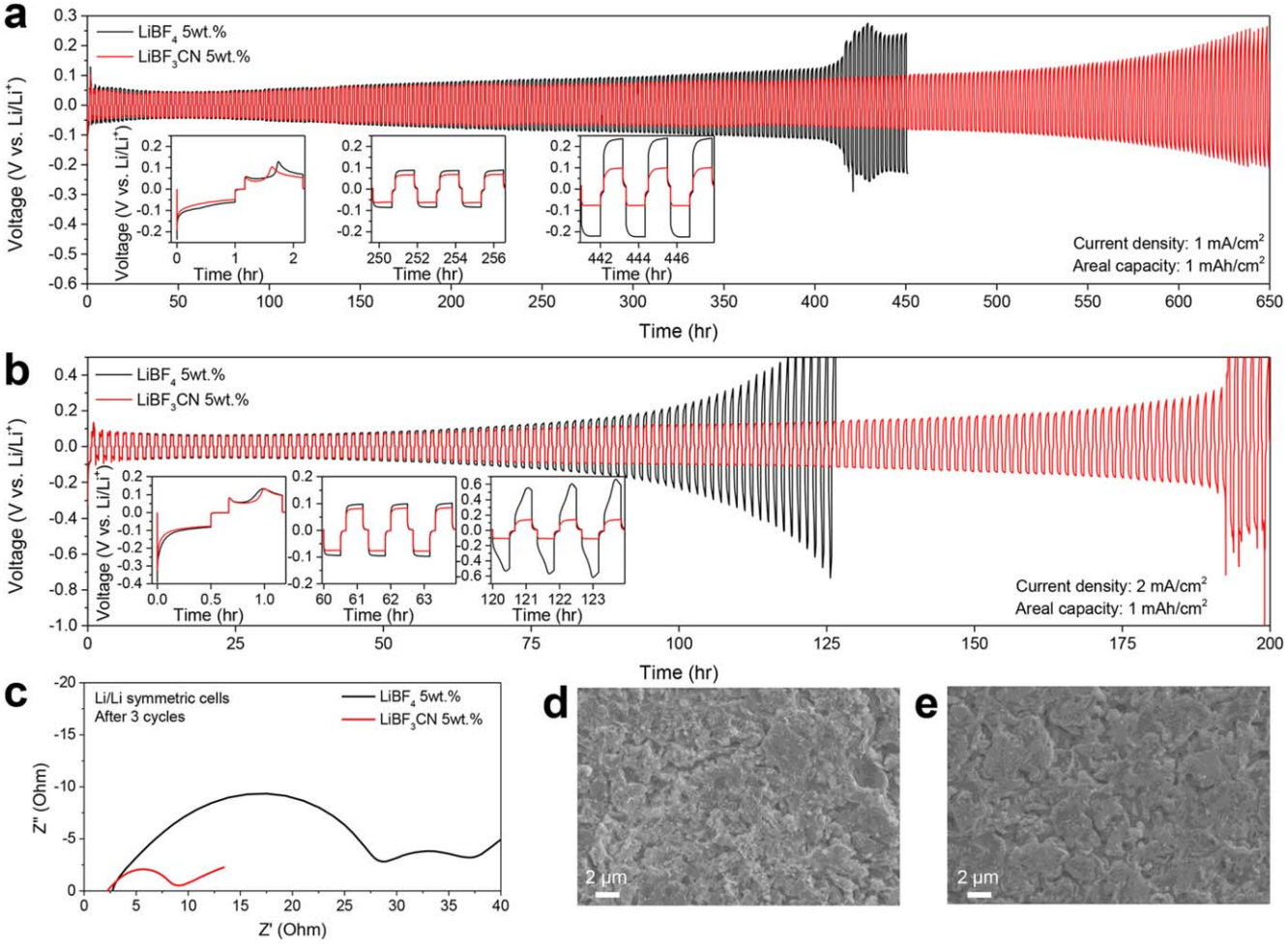

Figure 2. (a) Galvanostatic cycling results obtained for symmetric Li/Li cells using 5 wt% $LiBF_4$-containing electrolyte and 5 wt% $LiBF_3CN$-containing electrolyte at 1 mA cm^{-2} for 1 mAh cm^{-2}. The insets are the corresponding voltage profiles at 0, 250 and 440 h. (b) Galvanostatic cycling results obtained for symmetric Li/Li cells using 5 wt% $LiBF_4$-containing electrolyte and 5 wt% $LiBF_3CN$-containing electrolyte at 2 mA cm^{-2} for 1 mAh cm^{-2}. The insets are the corresponding voltage profiles at 0, 60 and 120 h. (c) EIS spectra of symmetric Li/Li cells after 3 cycles using 5 wt% $LiBF_4$-containing electrolyte and 5 wt% $LiBF_3CN$-containing electrolyte. (d) FE-SEM image of Li metal after 100 cycles at 1 mA cm^{-2} for 1 mAh cm^{-2} in symmetric Li/Li cells using 5 wt% $LiBF_4$-containing electrolyte. (e) FE-SEM image of Li metal after 100 cycles at 1 mA cm^{-2} for 1 mAh cm^{-2} in symmetric Li/Li cells using 5 wt% $LiBF_3CN$-containing electrolyte.

voltage profiles with higher overpotentials. It is expected that a critical problem in the cells with $LiBF_4$-containing electrolyte occurs after 100 cycles since a large increase in polarization is observed after 100 cycles. In addition, the rate performance and corresponding

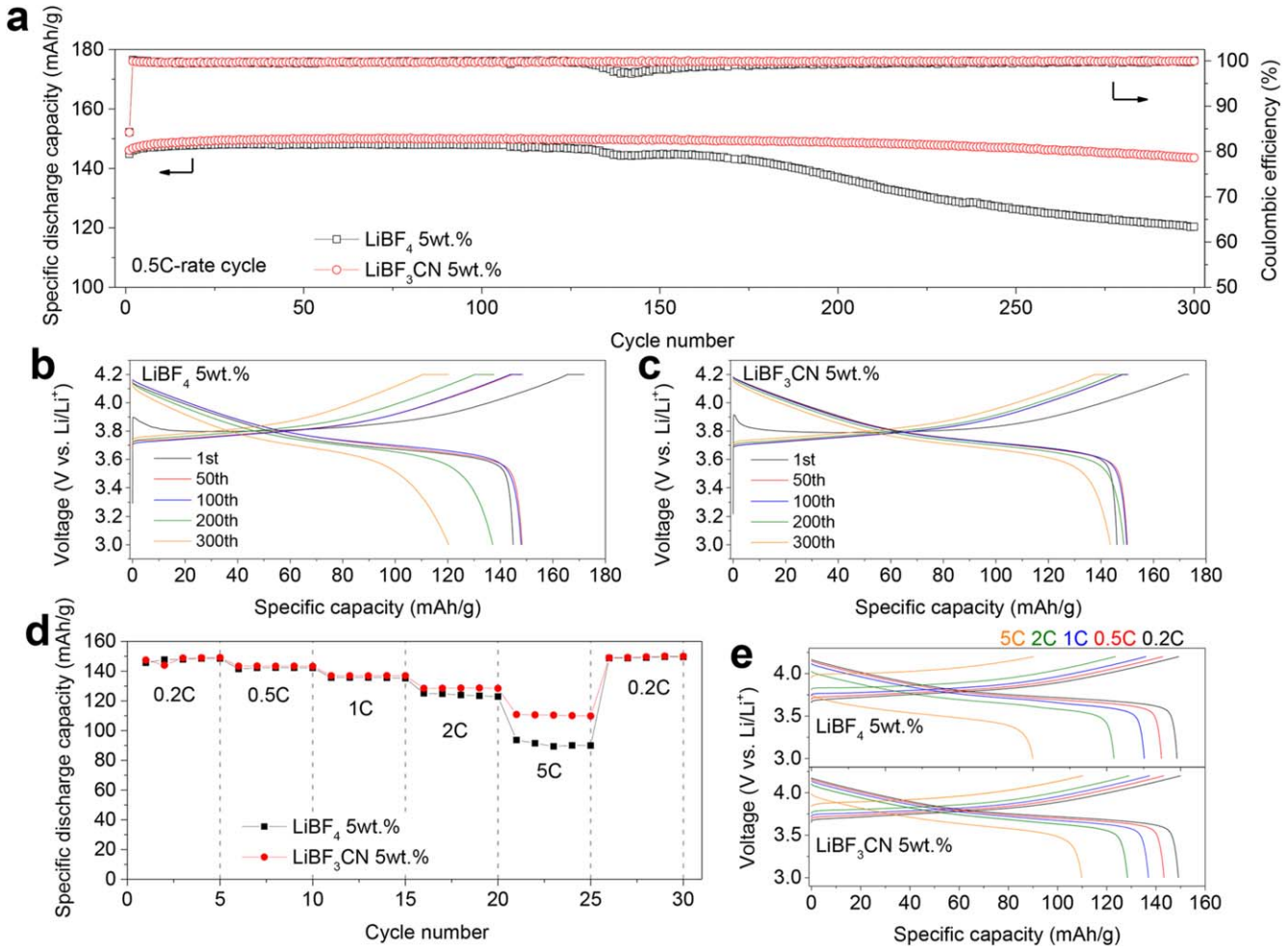

Figure 3. (a) Galvanostatic cycling results obtained for NCM523/Li cells using 5 wt% $LiBF_4$-containing electrolyte and 5 wt% $LiBF_3CN$-containing electrolyte. (b) Corresponding voltage profiles obtained for NCM523/Li cells using 5 wt% $LiBF_4$-containing electrolyte. (c) Corresponding voltage profiles obtained for NCM523/Li cells using 5 wt% $LiBF_3CN$-containing electrolyte. (d) Rate performance of NCM523/Li cells using 5 wt% $LiBF_4$-containing electrolyte and 5 wt% $LiBF_3CN$-containing electrolyte. (e) Corresponding voltage profiles of NCM523/Li cells using 5 wt% $LiBF_4$-containing electrolyte and 5 wt% $LiBF_3CN$-containing electrolyte.

voltage profiles of NCM523/Li cells between the two electrolyte systems are compared in Figs. 3d and 3e. Although the capacity difference is not very noticeable at low current densities such as 0.2, 0.5, 1 and 2 C, the cells with $LiBF_3CN$-containing electrolyte exhibit significantly improved rate performance at 5 C where the discharge capacities in the $LiBF_4$-containing electrolyte and in the $LiBF_3CN$-containing electrolyte are 89.9 and 109.8 mAh g^{-1}, respectively. The voltage hysteresis in the cells with $LiBF_3CN$-containing electrolyte at 5 C is significantly less compared to the cells with $LiBF_4$-containing electrolyte as shown in Fig. 3e.

Characterization of deposited lithium metal.—In an effort to understand the differences in the lithium deposition behavior between the $LiBF_4$-containing electrolyte and the $LiBF_3CN$-containing electrolyte, the deposited lithium morphologies and surface films on lithium metal were investigated by using FE-SEM and cryo-TEM after the first deposition at 1 mA cm^{-2} for 1 mAh cm^{-2}. In Figs. 4a and S4a, the deposited lithium metal in the $LiBF_4$-containing electrolyte has non-uniform mossy and needle-like dendrites. However, the lithium metal deposited from the $LiBF_3CN$-containing electrolyte (Figs. 4b and S4b) is observed to be comparatively smooth. The modified morphology of the deposited lithium in the $LiBF_3CN$-containing electrolyte can be attributed to the different SEI film formation by the preferentially decomposed $LiBF_3CN$ additive. Generally, the smooth lithium form is considered as more appropriate structure for stable cycling of lithium metal batteries than the sharp and narrow lithium morphology due to the favorable features such as suppressing dead lithium formation and inhibiting electrolyte decomposition during the lithium deposition/stripping cycling.[38,39] Furthermore, the smooth morphology of lithium deposition is more beneficial for battery safety since it can reduce the probability of dendrite penetration into the separators which can result in cell short circuit and thermal runaway.[2,40,41] Thus, the cycling improvement in the Li/Li and NCM523/Li cells with the $LiBF_3CN$-containing electrolyte as shown above can be attributed to the smooth lithium morphology. The difference of the thickness of the SEI on the deposited lithium metal for the two electrolyte systems is compared in Figs. 4c and 4d. Since the SEI is very sensitive to beam damage and temperature, cryo-TEM (−180 °C) provides more accurate information without sample damage.[42] Thus, imaging of the SEI was carried out using the cryo-TEM technique with careful inspection. The cryo-TEM images obtained from the deposited lithium metal in the $LiBF_4$−containing electrolyte reveals that a thick (≈40 nm) SEI film is formed on the lithium metal (Figs. 4c and S5a). However, much thinner SEI films (≈20 nm) are observed on the deposited lithium metal in the $LiBF_3CN$-containing electrolyte as shown Figs. 4d and S5b. This suggests that the different electrolyte additives result in the generation of different SEI thicknesses where the reductive decomposition of the $LiBF_3CN$ additive on lithium metal results in the generation of

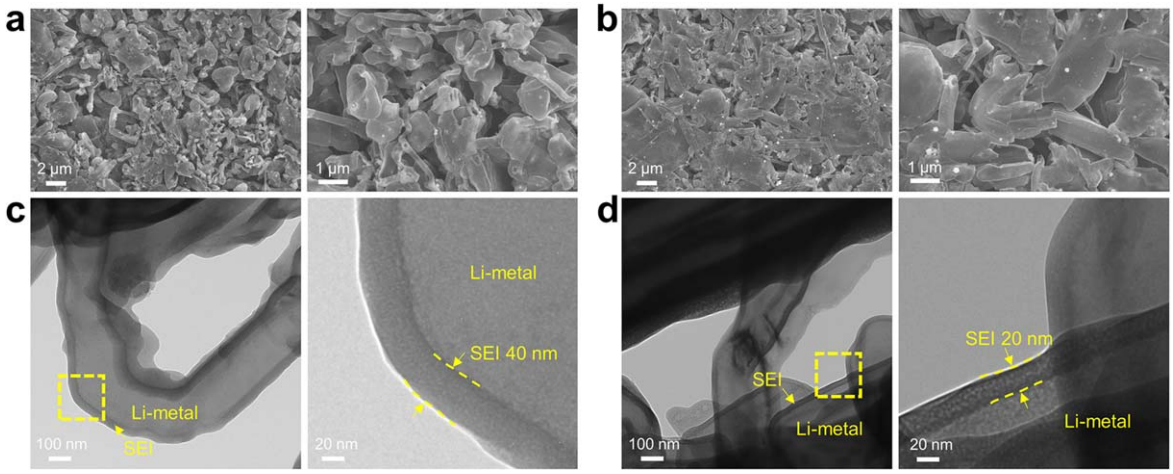

Figure 4. FE-SEM images of the deposited Li in (a) $LiBF_4$-containing electrolyte and (b) $LiBF_3CN$-containing electrolyte at 1 mA cm^{-2} for 1 mAh cm^{-2}. Cryo-TEM images of the deposited Li in (c) $LiBF_4$-containing electrolyte and (d) $LiBF_3CN$-containing electrolyte at 1 mA cm^{-2} for 1 mAh cm^{-2}.

a thin SEI. Generally, a thin SEI has lower resistance in which the lithium ion diffusion through the thin SEI is faster than that through a thick SEI.[5,43] Thus, the thin SEI formed on lithium metal in the $LiBF_3CN$-containing electrolyte can play an important role in improving the rate performance in addition to the decreasing the interfacial resistance.

XPS analysis was also employed to investigate the chemical composition of the SEI films generated on the deposited lithium metal in the two electrolyte systems, which are provided in Figs. 5, S6 and S7. In the C 1s spectra (Fig. 5a), both electrolyte systems contain peaks characteristic of $-CO_3$ (289.9 eV), $-C{=}O$ (288.4 eV) and C–O–C (286.5 eV)[44] consistent with the presence the commonly observed species such as lithium carbonate, lithium alkyl carbonates, carboxylates, and polyethers. However, for the $LiBF_3CN$-containing electrolyte, the C–O–C intensity is significantly diminished, consistent with a decrease in polymeric species in the SEI. In the F 1s spectra (Fig. 5b), both electrolyte systems have similar peaks in the range of 685–688 eV which can be deconvoluted into three components centered at 685, 687.1 and 687.5 eV, corresponding to LiF, B–F and $Li_xPO_yF_z$, respectively.[24,26,44] The O 1s and Li 1s spectra in Figs. 5c and S6 suggest that there is more Li_2O (258 eV in O 1s, 53.7 eV in Li 1s) present in the SEI of lithium deposited from the $LiBF_3CN$-containing electrolyte.[24,45] The B 1s spectra (Fig. S7) have similar peak trends including B–F and B–O in both electrolyte systems.[26] In the N 1s spectra as provided in Fig. 5d, two peaks characteristic of LiN_xO_y (399.9 eV) and Li_3N (398.6 eV) are observed only in the $LiBF_3CN$-containing electrolyte.[26] The XPS results suggest that the SEI film on deposited lithium in the $LiBF_3CN$-containing electrolyte contains N-compounds, more Li_2O and less polymeric species while the $LiBF_4$-containing electrolyte generates more polymeric species without N-compounds. The compositional differences of SEI between the two electrolyte systems can be ascribed to the presence of the novel electrolyte additive. During the lithium deposition, the reductive decomposition of $LiBF_3CN$ generates a dense and robust SEI film with N-compounds (LiN_xO_y, Li_3N) and Li_2O, which can prevent excessive decomposition of other organic electrolyte components, resulting in the generation of a thin SEI with less polymeric species. However, a dense and stable SEI film is not formed with the $LiBF_4$-containing electrolyte due to lack of the cyano group ($-CN$). Thus, a thick SEI film with more polymeric species is formed due to the continuous decomposition of organic electrolyte components. The polymeric SEI is softer and more porous than the inorganic SEI and the organic species in the polymeric SEI are more soluble in the electrolyte. The unfavorable features of polymeric SEI cause a high probability of SEI fracture and continuous side reactions of electrolyte, resulting in a low Coulombic efficiency and poor cycling stability.[46,47] However, LiN_xO_y and Li_3N are well-known as fast lithium ionic

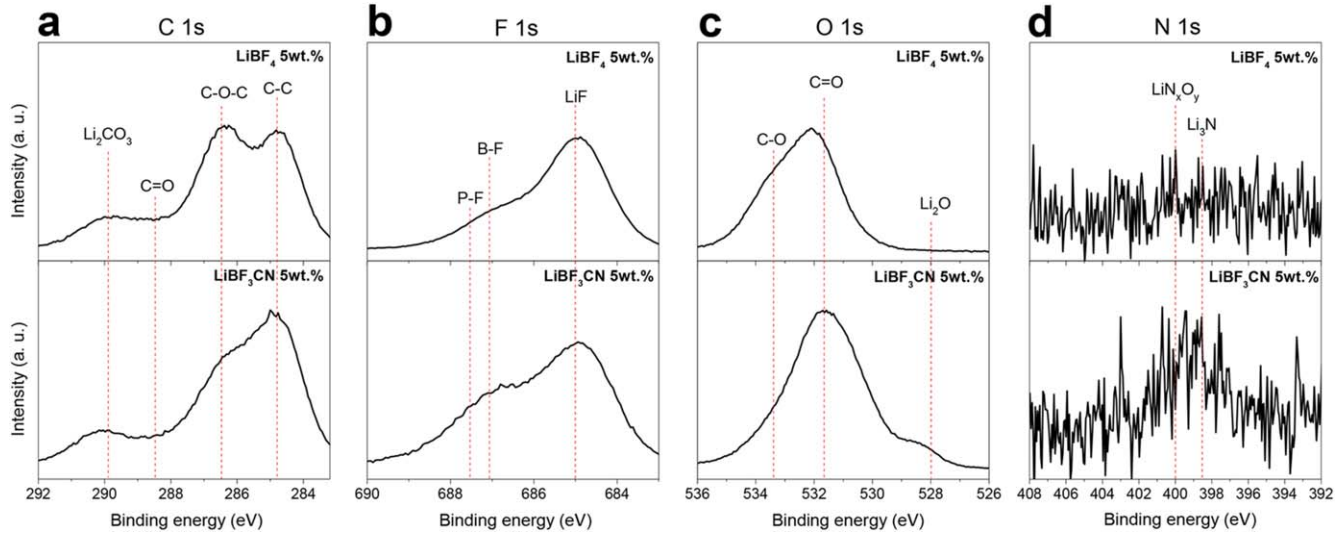

Figure 5. (a) C 1s, (b) F 1s (c) O 1s and (d) N 1s XPS spectra obtained from Li metal after 50 cycles using 5 wt% $LiBF_4$-containing electrolyte and 5 wt% $LiBF_3CN$-containing electrolyte at 1 mA cm^{-2} for 1 mAh cm^{-2}.

conductors[48–51] and thus beneficial SEI components. In addition, the Li_2O is beneficial for the generation of a robust and stable SEI by preventing excessive electrolyte decomposition.[52–54] Consequently, the N-compounds and Li_2O in the SEI derived from the $LiBF_3CN$ additive are critical components which decrease the resistance of the SEI affording stable lithium deposition/stripping and resulting in superior electrochemical performance.

Conclusions

A novel electrolyte additive, $LiBF_3CN$, has been synthesized and the effect of the novel additive for lithium metal batteries has been examined. The electrochemical tests using symmetric Li/Li cells and NCM523/Li cells demonstrate that the $LiBF_3CN$-containing electrolyte improves cycling stability and rate performance. The NCM523/Li cells with $LiBF_3CN$-containing electrolyte exhibit superior capacity retention with 98.4% after 300 cycles while the capacity retention in the $LiBF_4$-containing electrolyte degrades continuously during cycling. The improved electrochemical performance can be attributed the favorable role of the $LiBF_3CN$ electrolyte additive for lithium deposition behavior. The thin (≈20 nm) and robust SEI film including N-compounds (LiN_xO_y, Li_3N) and Li_2O derived from reductive decomposition of $LiBF_3CN$ affords stable lithium deposition/stripping with low resistance, resulting in significantly improved electrochemical performance.

Acknowledgments

This material is based upon work supported by the U.S. Department of Energy, Office of Science, EPSCoR National Laboratory Partnership Program, under Award Number DE-SC0021392.

ORCID

Venkata A. K. Adiraju https://orcid.org/0000-0001-6027-7288
Brett L. Lucht https://orcid.org/0000-0002-4660-0840

References

1. W. Xu, J. Wang, F. Ding, X. Chen, E. Nasybulin, Y. Zhang, and J.-G. Zhang, *Energy Environ. Sci.*, **7**, 513 (2014).
2. K. N. Wood, M. Noked, and N. P. Dasgupta, *ACS Energy Lett.*, **2**, 664 (2017).
3. S. Chen, F. Dai, and M. Cai, *ACS Energy Lett.*, **5**, 3140 (2020).
4. P. P. Paul et al., *Adv. Energy Mater.*, **11**, 2100372 (2021).
5. B. Horstmann et al., *Energy Environ. Sci.*, **14**, 5289 (2021).
6. J. Liu et al., *Nat. Energy*, **4**, 180 (2019).
7. D. Lu et al., *Adv. Energy Mater.*, **5**, 1400993 (2015).
8. D. Aurbach, E. Zinigrad, Y. Cohen, and H. Teller, *Solid State Ionics*, **148**, 405 (2002).
9. K. Xu, *Chem. Rev.*, **104**, 4303 (2004).
10. K. Xu, *Chem. Rev.*, **114**, 11503 (2014).
11. J. Xiao, *Science*, **366**, 426 (2019).
12. B. Wu, J. Lochala, T. Taverne, and J. Xiao, *Nano Energy*, **40**, 34 (2017).
13. O. B. Chae, J. Kim, and B. L. Lucht, *J. Power Sources*, **532**, 231338 (2022).
14. I. Yoon, S. Jurng, D. P. Abraham, B. L. Lucht, and P. R. Guduru, *Energy Storage Mater.*, **25**, 296 (2020).
15. C. V. Amanchukwu, Z. Yu, X. Kong, J. Qin, Y. Cui, and Z. Bao, *J. Am. Chem. Soc.*, **142**, 7393 (2020).
16. L.-P. Hou et al., *Angew. Chem. Int. Ed.*, **61**, e202201406 (2022).
17. E. Markevich, G. Salitra, F. Chesneau, M. Schmidt, and D. Aurbach, *ACS Energy Lett.*, **2**, 1321 (2017).
18. G. Salitra, E. Markevich, M. Afri, Y. Talyosef, P. Hartmann, J. Kulisch, Y.-K. Sun, and D. Aurbach, *ACS Appl. Mater. Interfaces*, **10**, 19773 (2018).
19. Z. L. Brown, S. Jurng, C. C. Nguyen, and B. L. Lucht, *ACS Appl. Energy Mater.*, **1**, 3057 (2018).
20. Z. L. Brown, S. Heiskanen, and B. L. Lucht, *J. Electrochem. Soc.*, **166**, A2523 (2019).
21. W. Li, H. Yao, K. Yan, G. Zheng, Z. Liang, Y.-M. Chiang, and Y. Cui, *Nat. Commun.*, **6**, 7436 (2015).
22. S. Jurng, Z. L. Brown, J. Kim, and B. L. Lucht, *Energy Environ. Sci.*, **11**, 2600 (2018).
23. L. Yu, S. Chen, H. Lee, L. Zhang, M. H. Engelhard, Q. Li, S. Jiao, J. Liu, W. Xu, and J.-G. Zhang, *ACS Energy Lett.*, **3**, 2059 (2018).
24. Z. L. Brown and B. L. Lucht, *J. Electrochem. Soc.*, **166**, A5117 (2018).
25. L. Qiao et al., *Chem. Sci.*, **9**, 3451 (2018).
26. X. Wang, S. Li, W. Zhang, D. Wang, Z. Shen, J. Zheng, H. L. Zhuang, Y. He, and Y. Lu, *Nano Energy*, **89**, 106353 (2021).
27. H. Dai, X. Gu, J. Dong, C. Wang, C. Lai, and S. Sun, *Nat. Commun.*, **11**, 643 (2020).
28. O. B. Chae, V. A. K. Adiraju, and B. L. Lucht, *ACS Energy Lett.*, **6**, 3851 (2021).
29. S. Zhang, K. Xu, and T. Jow, *J. Solid State Electrochem.*, **7**, 147 (2003).
30. S. S. Zhang, K. Xu, and T. R. Jow, *J. Electrochem. Soc.*, **149**, A586 (2002).
31. M. Ue, *J. Electrochem. Soc.*, **141**, 3336 (1994).
32. M. Ue, A. Murakami, and S. Nakamura, *J. Electrochem. Soc.*, **149**, A1385 (2002).
33. X. Zuo, C. Fan, J. Liu, X. Xiao, J. Wu, and J. Nan, *J. Electrochem. Soc.*, **160**, A1199 (2013).
34. T. Livinghouse, *Org. Synth.*, **60**, 126 (1981).
35. S. Brownstein and G. Latremouille, *Can. J. Chem.*, **56**, 2764 (1978).
36. K. Bläsing, S. Ellinger, J. Harloff, A. Schulz, K. Sievert, C. Täschler, A. Villinger, and C. Zur Täschler, *Eur. J. Inorg. Chem.*, **2016**, 1175 (2016).
37. E. Bernhardt and H. Willner, *Z. Anorg. Allg. Chem.*, **635**, 2511 (2009).
38. J. Zheng, M. S. Kim, Z. Tu, S. Choudhury, T. Tang, and L. A. Archer, *Chem. Soc. Rev.*, **49**, 2701 (2020).
39. J.-H. Cheng, A. A. Assegie, C.-J. Huang, M.-H. Lin, A. M. Tripathi, C.-C. Wang, M.-T. Tang, Y.-F. Song, W.-N. Su, and B. J. Hwang, *J. Phys. Chem. C*, **121**, 7761 (2017).
40. M. Rosso, C. Brissot, A. Teyssot, M. Dollé, L. Sannier, J.-M. Tarascon, R. Bouchet, and S. Lascaud, *Electrochim. Acta*, **51**, 5334 (2006).
41. H. Wu, D. Zhuo, D. Kong, and Y. Cui, *Nat. Commun.*, **5**, 5193 (2014).
42. Y. Li et al., *Science*, **358**, 506 (2017).
43. X. Shen, R. Zhang, X. Chen, X.-B. Cheng, X. Li, and Q. Zhang, *Adv. Energy Mater.*, **10**, 1903645 (2020).
44. S. Liu, Q. Zhang, X. Wang, M. Xu, W. Li, and B. L. Lucht, *ACS Appl. Mater. Interfaces*, **12**, 33719 (2020).
45. K. Kanamura, H. Tamura, S. Shiraishi, and Z. i Takehara, *J. Electrochem. Soc.*, **142**, 340 (1995).
46. R. Mogensen, D. Brandell, and R. Younesi, *ACS Energy Lett.*, **1**, 1173 (2016).
47. J. Wang, W. Huang, A. Pei, Y. Li, F. Shi, X. Yu, and Y. Cui, *Nat. Energy*, **4**, 664 (2019).
48. U. v Alpen, A. Rabenau, and G. H. Talat, *Appl. Phys. Lett.*, **30**, 621 (1977).
49. Y. Kowada, M. Tatsumisago, and T. Minami, *Solid State Ionics*, **180**, 462 (2009).
50. W. Qi, L. Ben, H. Yu, Y. Zhan, W. Zhao, and X. Huang, *J. Power Sources*, **424**, 150 (2019).
51. X.-Q. Zhang, X. Chen, X.-B. Cheng, B.-Q. Li, X. Shen, C. Yan, J.-Q. Huang, and Q. Zhang, *Angew. Chem. Int. Ed.*, **57**, 5301 (2018).
52. B. D. Adams et al., *Nano Energy*, **40**, 607 (2017).
53. J.-Y. Hwang, S.-J. Park, C. S. Yoon, and Y.-K. Sun, *Energy Environ. Sci.*, **12**, 2174 (2019).
54. S. Li, W. Zhang, Q. Wu, L. Fan, X. Wang, X. Wang, Z. Shen, Y. He, and Y. Lu, *Angew. Chem. Int. Ed.*, **59**, 14935 (2020).